Ray-tracing the 8 July 2014 hail storm in Sofia, Bulgaria

Martin Slavchev[1,2*], Elzbieta Lasota[3], Jan Kapłon[3]

*[1]National Institute of Meteorology and Hydrology,
Tsarigradsko shose 66, 1784 Sofia, Bulgaria
[2] Faculty of Physics, Sofia University "St. Kliment Ohridski," Sofia, Bulgaria
[3]Institute of Geodesy and Geoinformatics , Wroclaw University of Environment and Life Sciences,
Wroclaw, Poland*

Abstract: In recent decades, the increase in the number and intensity of severe meteorological phenomena has been an indisputable trend worldwide. This is the reason why they are the subject of increased scientific interest. Globally, 2014 is characterized by many extreme phenomena that have caused huge economic losses. The geographical location and the diverse terrain of Bulgaria characterize it as one of the countries with intense thunderstorms and hail. West Bulgaria is the region with the highest frequency of thunderstorms in the country, as well as other events with a high degree of impact, including hail, torrential rains and strong wind storms. This paper presents the application and analysis of Slant Total Delay (STD) obtained from the global navigation satellite system via Ray-tracing method from the Weather Research and Forecasting - Numerical Weather Prediction model for the severe hail storm over Sofia on 8 July 2014. The results of the numerical model are analyzed and compared with the observed Slant Total Delays from the GNSS network. The development of a modern and reliable approach for nowcasting of severe meteorological events is of paramount importance for operational weather forecasters worldwide.

Keywords*:* nowcasting, numerical weather experiments, convective precipitation, hail, slant total delay, zenith total delay, raytracing**.**

1. INTRODUCTION

Bulgaria's geographical location and diverse terrain characterize the high frequency and intensity of thunderstorms and hail events. Like in many other countries, the frequency and severity of hail storms and heavy rains increased in Bulgaria in the past decade (Bocheva et. al., 2018). West Bulgaria is the region with the highest frequency of thunderstorms in the country (Bocheva et al., 2013) and the highest in Europe

---

* martin.slavchev@meteo.bg

(Taszarek et al. 2019). Other high impact weather events include hailstorms, torrential precipitations, and severe convectively-induced wind storms (Zamfirov et al., 2014; Gospodinov et al., 2015; Bocheva and Simeonov, 2015). In line with these trends, a series of flash floods were registered during the warm half of 2014 (Stoycheva et. al, 2015; Mircheva et al., 2020).

The synoptic environment for the day of the severe hail storm in Sofia, and all supercell storms in Bulgaria on July 8, 2014, is described and analysed by Bocheva et. al., (2018). The extreme hail event, accompanied by a strong wind gust, heavy rain, and high lightning frequency was registered between 13:30 UTC and 14:00 UTC. The giant hailstones had a diameter up to 10 cm and irregular shape.

Guerova et al., (2019) analyses the supercell storms developed over the Sofia plain on 8 July 2014 using GNSS derived water vapour. The temporal variability of integrated water vapour (IWV) has continuously increased before the supercell formation between 04:00 and 11:00 UTC. The flash rate increased from 11:00 UTC and peaked at 12:28 UTC. Between 11:00 and 12:28 UTC, the IWV peaked at 29 kg/m^2 40 min before the flash rate peak. After the hail storm, the IWV high values were above the monthly threshold. IWV values remained high with the storm dissipation (Guerova et al., 2019).

In the last few decades, the application of GNSS Slant Total Delay for monitoring of the atmosphere is becoming more and more applicable. In particular, the Slant Total Delay (STD) has been used for Numerical Weather Prediction (NWP) model validation (Haan et al. 2002 , Bender et al. 2008), STD assimilation (Kawabata et al., 2013) and also for multi-model dataset (GFS/WRF/ERA) evaluation during a tropical cyclone (Lasota et al. 2020).

This paper presents the application and analysis of STD obtained from global navigation satellite system (GNSS) and via ray-tracing technique from the Weather Research and Forecasting (WRF) Numerical Weather Prediction model for the severe hail storm over Sofia on 8 July 2014. The aim of the paper is to evaluate the NWP model skills in the representation of the spatiotemporal variation of humidity, temperature, pressure and water vapour before, during and after the storm.

2. METHOD OF APPROACH AND USED DATA SETS

2.1 Numerical weather prediction model

WRF Model is a state-of-the-art mesoscale NWP system designed for both atmospheric research and operational forecasting applications. It has two dynamical cores, a data assimilation system, and a software architecture supporting parallel computation and system extensibility. The effort to develop WRF began in the latter 1990's and was a collaborative partnership of the National Center for Atmospheric Research, the National

Oceanic and Atmospheric Administration (represented by the National Centers for Environmental Prediction and the Earth System Research Laboratory), the U.S. Air Force, the Naval Research Laboratory, the University of Oklahoma, and the Federal Aviation Administration. In this study, we exploited the 3.7.1 version of the WRF model, which is installed and compiled on the cluster in the Faculty of Physics, Sofia University "St. Kliment Ohridski".

This WRF model is non-hydrostatic and with no data assimilation. The initial and boundary conditions are from the Global Forecast System (GFS). Meteorological data in the model is provided 24 hours in advance at 44 irregularly spaced levels up to 20 km. The WRF model consists of 3 domains, two of which are nested, with a horizontal resolution of 18, 6 and 3 km, respectively, presented in Figure 1. In this study, we performed two different experiments based on the cumulus parameterization scheme, which are summarized in Table 1.

Table 1. Experiment 1 and 2 for both stations SOFI and SOF1

Experiment	Station name	WRF Cumulus Parameterisation
WRF-KF SOFI and SOF1 Kain-Fritsch Scheme		
WRF-NCP	SOFI and SOF1	No Cumulus scheme

The used WRF model encompass following setups:

1) Cumulus Parameterization:
  - Kain-Fritsch scheme: A deep and shallow sub-grid scheme using a mass flux approach with downdrafts and CAPE removal time scale - (KF)
  - No Cumulus Scheme - (NCP)

2) Microphysics: A sophisticated 5-class scheme that has ice, snow and graupel processes, suitable for real-data high-resolution simulations. Includes ice sedimentation and time-split fall terms. Reference: Lin, Farley and Orville (1983, JCAM); Rutledge and Hobbs (1984); Tao et al. (1989), Chen and Sun (2002).

3) Longwave radiation: Rapid Radiative Transfer Model - (Mlawer et al., 1997);

4) Shortwave radiation: Goddard shortwave: two-stream multi-band (8) scheme with ozone from climatology and cloud effects. Increases computational time (3x) at radiation call times. Ozone profile is a function of season and region (tropics, mid-latitude, polar). Fixed CO_2. (Chou and Suarez 1994).

5) Land-surface model: Noah Land Surface Model (Chen et al., 1996);

6) Planetary boundary layer: Yonsei University scheme (Hong et al., 2006);

Fig. 1. Domains used in the WRF model version 3.7.1

2.2 Ray-tracing method

The GNSS signal path in any arbitrary direction can be simulated from meteorological data, especially from those stored in NWP models, applying a ray-tracing method. Consequently, the ray-tracing allows calculating the STD (Slant Total Delays) along the way between the satellite and ground-based receiver. In this study, we follow the methodology applied by Lasota et al. (2020) and use the 2D piecewise linear ray-tracing tool, which is one of the simplest, but computationally efficient and accurate ray-tracing approach. In the 2D methods, the horizontal gradients of refractivity are neglected since they are significantly smaller compared to vertical gradients. This assumption implies that the GNSS signal does not leave the plane of the constant azimuth (A).

Given the azimuth and elevation angle (**ea**) between a station and the satellite, the ray-path is modelled iteratively following the linear segments (s_1, s_2, s_3, ...s_n) linking the station and the satellite. Figure 2 demonstrates the schematic geometry of the applied algorithm (adopted from Lasota et al., 2020). More details about the used ray-tracing algorithm can be found in the works of Hobiger et al. (2008), Hofmeister (2016), and Lasota et al. (2020).
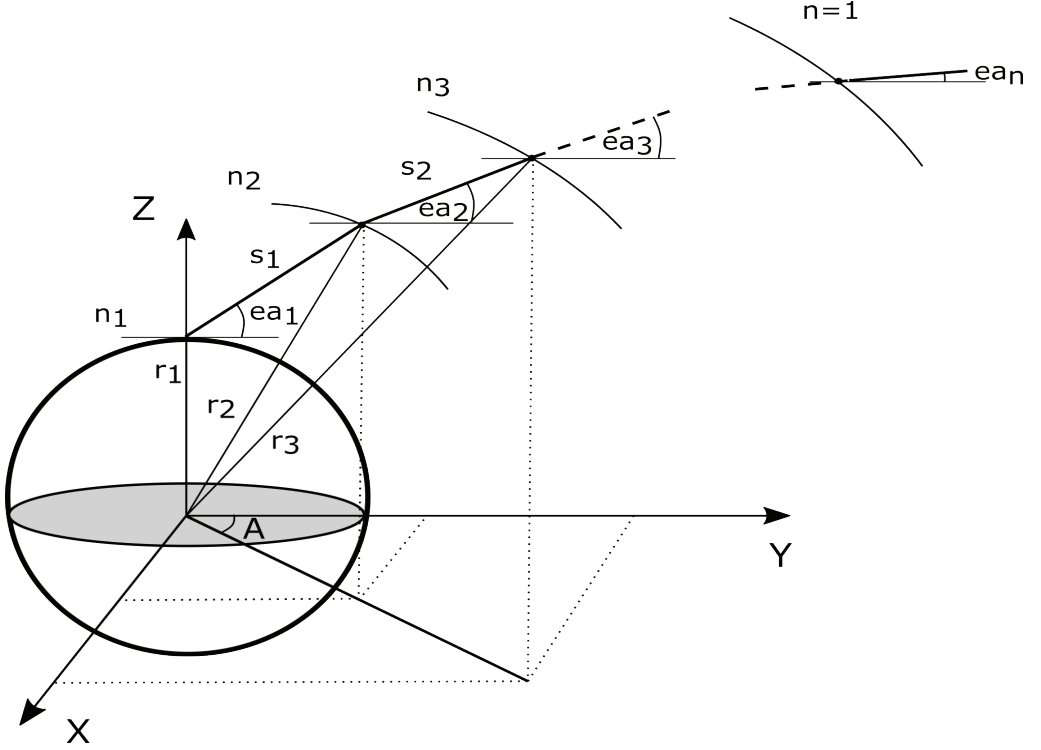
Fig. 2. The geometry of the 2D linear piecewise ray-tracing approach. The variables used are the tangential radius from the Earth's centre, **r**, the elevation angle, **ea**, the geometric distance between two adjacent ray-points, **s**, and the refractive index at specified height levels, **n**. The figure is adopted from Lasota et al. (2020).

In order to reconstruct the signal path, the 3D refractivity (N) field must be computed based on the basic meteorological parameters provided in weather models: temperature (T, in °K), pressure (P, in hPa) and the partial pressure of water vapour (e, in hPa). The refractivity is dependent on the signal's frequency, hence, for the GNSS signal valid is the formula demonstrated by Davis et al. (1985):

$$N = k_1 R_d \left(\frac{P - e}{R_d T} + \frac{e}{R_w T}\right) + \left(k_2' \frac{e}{T} + k_3 \frac{e}{T^2}\right)$$

where k_1, $k_2' = k_2 - k_1(R_d - R_w)$ and k_3 denotes the physical constants, here "the best available" taken from Rueger, R_d and R_w are the specific gas constants for dry air and water vapour, respectively.

Since the focus of this study is put on the hail and to ensure the high precision, the influence of hydrometeors on propagating GNSS signal is calculated as:

$$N_{hm} = N_{lw} + N_{ice} \approx 1.45 \cdot LWC + 0.69 \cdot IWC,$$

where N_{lw} and N_{ice} represent the refractivity of liquid and solid water particles, *LWC* and *IWC* are the liquid and ice water contents in g/cm^3. However, meteorological variables stored in WRF model does not include *LWC* and *IWC*, which must be computed from the available rain, cloud, snow, and graupel mixing ratios employing pressure, water vapour partial pressure and temperature.

Finally, STD values are assessed by the integration of the mean refractivity values **n** in line segments **s** (Fig. 2) along the way between the station and neutral atmosphere (level **k**):

$$STD = \sum_{i=1}^{k-1} [(n-1)s_i]$$

The resulting STD can be divided into hydrostatic (*SHD*), wet (*SWD*) and hydrometeors (*SHmD*) components:

$$STD = SHD + SWD + SHmD.$$

Furthermore, the hydrostatic part encompasses the accumulated bending effect along the ray-path, which can be calculated according to the equation:

$$g_{bend} = \sum_{i=1}^{k-1} [(s_i - cos(ea_i - ea_k)) \cdot s_i],$$

where ea_i is the actual elevation angle at each ray point and ea_k is the outgoing elevation angle at the final height level.

2.3 GNSS STD Estimation - Bernese 5.2 WUELS method

In this study, we followed the procedure described in Lasota et al. (2020) and processed GNSS observations using Bernese 5.2 software in precise point positioning (PPP) mode with a cutoff angle of 3°. From all available satellite systems, only GPS observations were used. STD and gradients were calculated with a temporal resolution of 15 min and 1 h, respectively.

STDs were determined for each observation between a satellite and receiver by adjusting ZTD together with tropospheric linear horizontal gradients, which reflect the first-degree asymmetry of the troposphere. Basically, the ZTD can be divided on hydrostatic (zenith hydrostatic delay (ZHD)) and wet (zenith wet delay (ZWD)) components. However, external information is needed to assess ZHD since GNSS observations do not include information about the contribution of the aforementioned dry and wet parts. The most common way to accurately estimate ZHD is using the Saastamoinen model (Saastamoinen et al., 1972). Afterwards, the transformation between delays in the zenith and satellite directions can be achieved using separate mapping functions for hydrostatic (*mfh*) and wet (*mfw*) delays and horizontal gradient

(*mfg*) components. In this study, we applied the Vienna mapping function for hydrostatic and wet delays and mapping functions proposed by Chen and Herring (G. Chen, T.A. Herring, 1997) for horizontal gradients. Since horizontal gradients represent only first-order anisotropy of the troposphere and may not reflect all atmospheric horizontal variability, postfit phase residuals (RES) must be evaluated together with other parameters. Eventually, the GNSS delays towards the satellite can be written as:

STD_GNSS(*ea, az*) = ZHD·*mfh*(*ea*) + ZWD·*mfw*(*ea*) + *mfg*(*ea*)·(GN·cos(*az*) + GE·sin (*az*)) + RES(*ea, az*),

where GN and GE are north-south and east-west gradient components, **az** is the azimuth, **ea** is the elevation angle, and *mfg*(*ea*) = 1/(sin (*ea*)·tan (*ea*)) + *C*, with *C* = 0.0032.

2.4 GNSS stations: SOFI and SOF1

SOFI:

For the severe hail case study in Sofia on 08 July 2014, the only freely available Rinex data is for station SOFI, which is a part of the International GNSS Service (IGS) network. SOFI is situated southeast of Sofia city in Plana mountain at an altitude of 1119.6 m above sea level (asl) and with coordinates 42°55'N and 23°29'E (left panel in Figure 3).

SOF1:

Station SOF1 is a private GNSS network station. The data for this station is provided by the private company: "1Yocto", which has an RTK network for PPP in Bulgaria. SOF1 station is situated in the south-east part of Sofia city (42.65°N and 22.36°E) at an altitude of 650.6 m asl , which is shown in the right panel of Figure 3. The station is closer to the area affected by the severe hail storm, however, it is in an urban, highly populated district with dense infrastructure.

3. RESULTS

3.1. Fractional STD error for stations SOFI and SOF1

The daily mean fractional STD differences are computed by subtracting GNSS-STD and STD values using WRF-NC and WRF-KF divided by GNSS-STD. For the period 07 - 09 July 2014 for station SOFI the fractional STD is positive and it is between 0.25% and 0.40%. On 7 and 8 July 2014, the fractional STD for SOF1 station was in the range ±0.20%, while on 09 July 2014 there is a strong positive fractional error at above 0.50%. Thus it can be concluded that the WRF-STD at the location of SOF1 station is better simulated in comparison to WRF-STD at SOFI station on 7 and 8 July but not for

9 July. In addition, the two experiments WRF-KF (green bars on figure 4) and WRF-NCP (blue bars on figure 4) tend to have similar fractional error with a slightly lower error for WRF-KF.
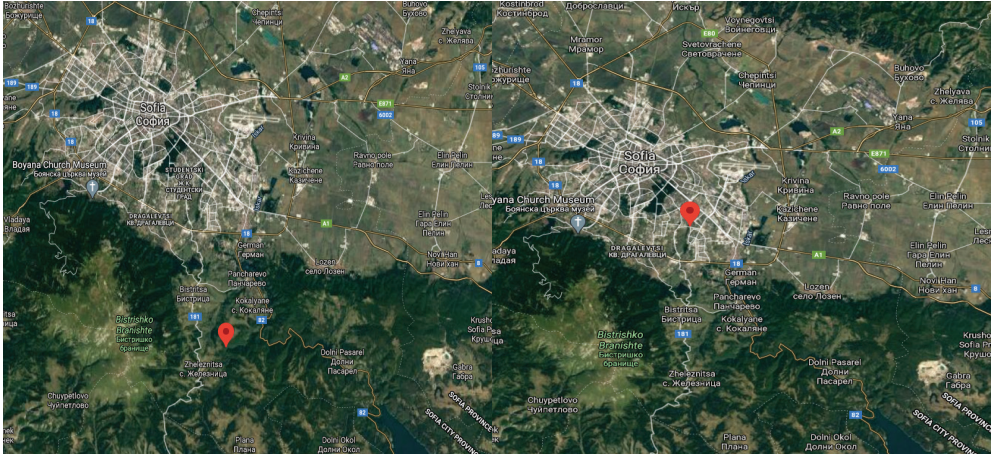

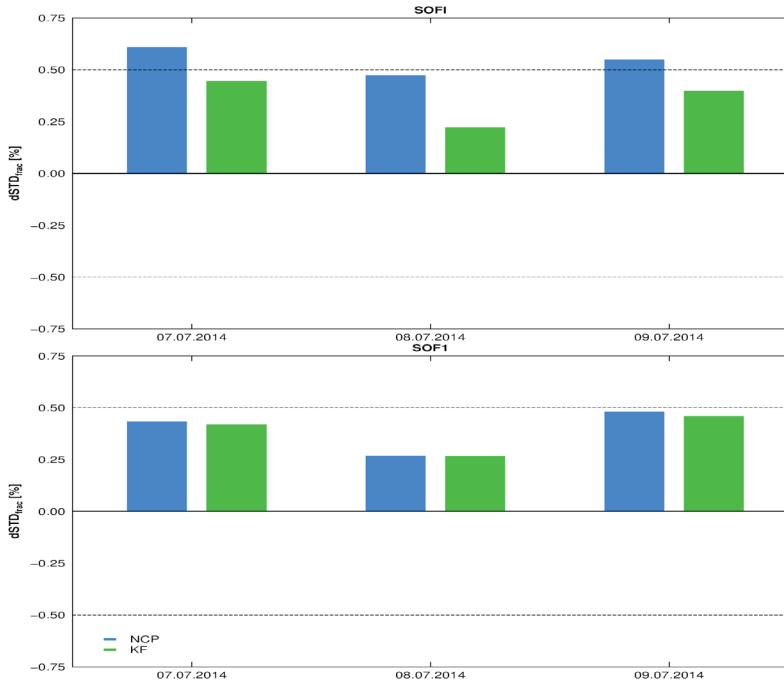**Fig. 3.** Location of SOFI (left) and SOF1 (right) stations. Images taken from Google Maps.

Fig. 4. Fractional error of daily mean STD for: KF (green) and NCP (blue) at SOFI (top) and SOF1 (bottom) stations from 7 to 9 July 2014.

3.2. WRF-KF and WRF-NCP STD for station SOFI: 7 - 9 July 2014.

The fractional error of STD, presented in figure 5, is with temporal resolution 15 min. The overall positive fractional STD error ranges from 0.25% up to 2% for both parameterisation experiments. At the time of the hail storm at around 13:00 UTC there is a good agreement between GNSS and WRF-KF. However there is a clearly visible negative pick, followed by a strong positive one. Possible explanation is a shift by phase between WRF and GNSS due to the rapid development of the hail storm. Overall for both KF and NCP the model is underestimating the STD.
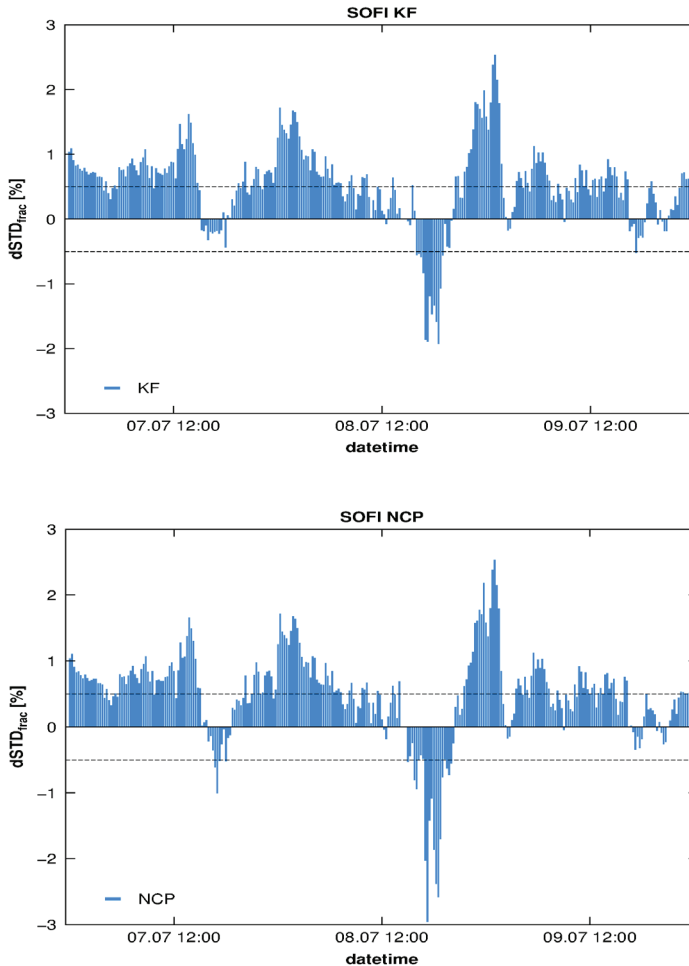
Fig. 5. Fractional STD error with temporal resolution 15 min between WRF-KF (top) and WRF-NCP (bottom) and GNSS for the period 7-9 July 2014 from SOFI station in Bulgaria.

3.3. WRF-KF and /WRF-NCP STD for station SOF1: 7 to 9 July 2014.

The fractional error of STD, presented in figure 6, is with temporal resolution 15 min and is derived by: 1) subtracting WRF-KF/WRF-NCP from GNSS STD and 2) dividing by GNSS STD. For station SOF1 negative and positive errors are almost equally spread. At the time of the hail storm at around 12:30 UTC there is negative error at around 0.11% followed by a negative pick up to 2%. After the negative error there is again the large positive pick up to 2% for WRF-KF and 1.6% for WRF-NCP. Possible explanation is not only the shift by phase between WRF and GNSS due to the rapid development of the hail storm, but also the influence of the city infrastructure. Before the hail storm and during the event for both KF and NCP the model is overestimating the values of STD.
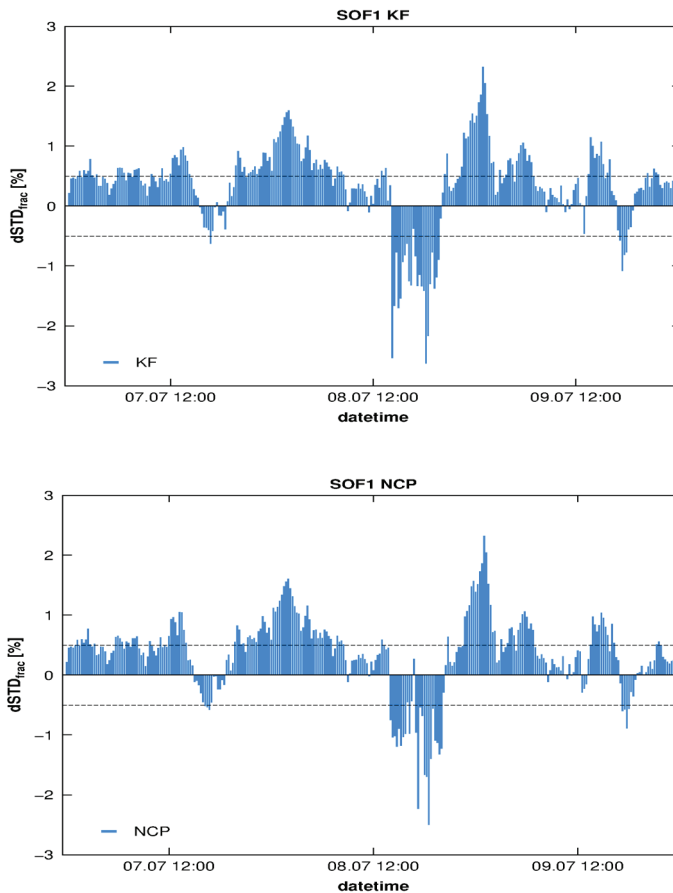
Fig. 6. Fractional error with temporal resolution 15 min between STD WRF-KF (top) and WRF-NCP (bottom) and GNSS for the period 7-9 July 2014 from SOF1 station in Bulgaria.

3.4. Hail storm 8 July 2014.

The fractional error of STD, presented in figure 7a and 7b, is for 8 July 2014. Overall both WRF-KF and WRF-NCP underestimate the STD before the hail storm. WRF-KF has better agreement during the event with almost 0% fractional error, meaning that observed and calculated STD values are almost the same. However after the event there are the same picks, first strong negative followed by strong positive ranging up to ±1.8%. Possible explanation is the shift by phase between GNSS and WRF due to the rapid advection of new air mass after the storm passage.
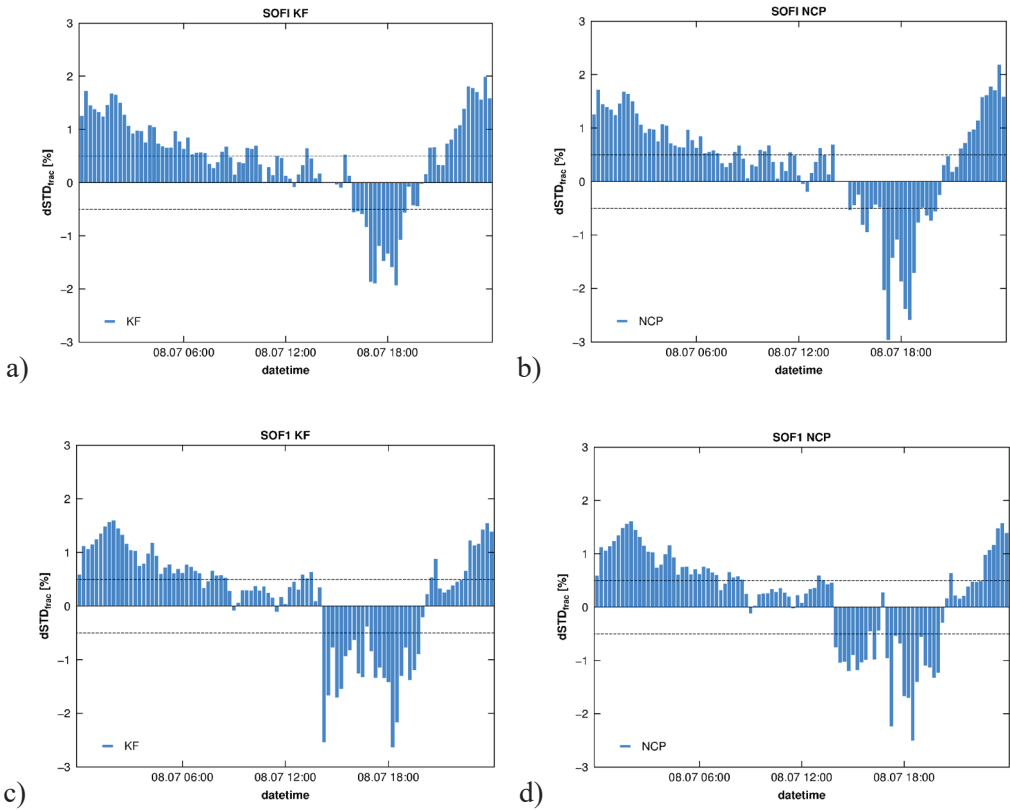

Fig. 7. Fractional error with temporal resolution 15 between STD calculated from WRF-KF (left) and WRF-NCP (right) and GNSS-STD for the day of the hail storm from SOFI (top) and SOF1 (bottom) station in Bulgaria.

The fractional error of STD, presented in figure 7c and 7d, is with temporal resolution 15 min and it is derived from subtracting WRF-KF/WRF-NCP from GNSS and it is divided by GNSS. Overall both WRF-KF and WRF-NCP overestimate the STD before, during and after the hail storm. However after the event there are the same picks, first strong negative followed by strong positive ranging up to ±2%. The model overestimates

the diurnal cycle of the STD. Possible explanation is the shift by phase between GNSS and WRF due to the rapid changes of the atmospheric conditions after the storm passage and the model weakness in simulation of post storm environment.

4. CONCLUSION

The high temporal resolution of 15 min for the STD provides important information about the state of the accessible water vapour in the atmosphere. There is a large bias in STD values for both stations between model and observed values. The WRF model clearly overestimates the STD values in the diurnal cycle for the whole period, not only the day of the storm. In terms of parameterisation, the Kain-Fritsch scheme is slightly less biased than the No Cumulus Scheme. Overall during the severe hail event in Sofia the agreement between calculated and observed data is good. However station SOFI is not representative enough for the hail case study, because it is in high altitude and south west from Sofia city. Large positive deviation in STD for both parameterizations, two hours after the convective storm is registered. The rapid development of the storm cell is not presented appropriately by the WRF model, which leads to the possible change in phase. For future work a combination between instability indexes, additional parameterization schemes for the WRF diurnal cycle and additional GNSS stations could improve the representation of the model STD.

ACKNOWLEDGEMENTS

REFERENCES

Baelen, J. V., M. Reverdy, F. Tridon, L. Labbouz, G. Dick, M. Bender, and M. Hagen, On the relationship between water vapour field evolution and the life cycle of precipitation systems, Q. J. R. Meteorol. Soc., 137(S1), 204-223, doi:10.1002/qj.785, 2011.

Bender Michael, Dick Galina, Wickert Jens, Schmidt Torsten , Song Shuli, Gendt Gerd, Ge Maorong, Rothacher Markus. (2008). Validation of GPS slant delays using water vapour radiometers and weather models. Meteorologische Zeitschrift. 17. 807-812. 10.1127/0941-2948/2008/0341.

Bocheva L. and Simeonov P., 2015: Spatio-temporal variability of hailstorms for Bulgaria during the period 1961–2010. 15th International Multidisciplinary Scientific GeoConference SGEM 2015, ISBN 978-619-7105-38-4 / ISSN 1314-2704, June 18-24, 2015, Book4, 1065–1072.

Bocheva Lilia, Dimitrova Tsvetelina, Penchev Rosen, Gospodinov Ilian, Simeonov Petio. (2018). Severe convective supercell outbreak over western Bulgaria on July 8, 2014. Időjárás. 122. 177-202. 10.28974/idojaras.2018.2.5.

Brenot, H., et al., A GPS network for tropospheric tomography in the framework of the Mediterranean hydrometeorological observatory cevennes-vivarais (southeastern France), Atmos. Meas. Tech., 7, 553-578, doi:10.5194/amt-7-553-2014, 2014.

G. Chen and T. A. Herring (1997), "Effects of atmospheric azimuthal asymmetry on the analysis of space geodetic data," J. Geophys. Res., Solid Earth, vol. 102, no. B9, pp. 20489–20502.

Chen F., Mitchell K., Schaake J., Xue Y., Pan H. L., Koren V., ... and Betts A. (1996) Modeling of land surface evaporation by four schemes and comparison with FIFE observations, Journal of Geophysical Research: Atmospheres, 101 (D3), 7251-7268.

Davis J., Herring T., Shapiro I., Rogers A., and Elgered G. (1985), Geodesy by radio interferometry: Effects of atmospheric modeling errors on estimates of baseline length, Radio science, vol. 20, no. 6, pp. 1593–1607.

E. Lasota, W. Rohm, G. Guerova and C. Liu (2020), A Comparison Between Ray-Traced GFS/ WRF/ERA and GNSS Slant Path Delays in Tropical Cyclone Meranti, IEEE Transactions on Geoscience and Remote Sensing, vol. 58, no. 1, pp. 421-435, Jan. 2020, doi: 10.1109/ TGRS.2019.2936785.

J. Saastamoinen (1972), Atmospheric correction for the troposphere and stratosphere in radio ranging satellites, in The Use of Artificial Satellites for Geodesy, vol. 15. Washington, DC, USA: American Geophysical Union, pp. 247–251.

Haan Siebren, Marel Hans, Barlag S. (2002), Comparison of GPS slant delay measurements to a numerical model: Case study of a cold front passage. Physics and Chemistry of the Earth, Parts A/B/C. 27. 317-322. 10.1016/S1474-7065(02)00006-2.

Hong Z., Campbell A. M., Coombs T. A. (2006), Numerical solution of critical state in super-conductivity by finite element software, Superconductor Sci and Tech, 19(12), 1246.

Gospodinov I., Dimitrova Ts., Bocheva L., Simeonov P., and Dimitrov R. (2015), Derecho-like event in Bulgaria on 20 July 2011. Atmos. Res. 158, 254–273.

Graham E., E. N. Koffi, and C. Matzler (2012), An observational study of air and water vapor convergence over the western Alps during summer and the development of isolated thunderstorms, Meteorologishe Zeitschrift, 21, 1-13.

Guerova G., T. Simeonov and N. Yordanova (2014), The Sofia university atmospheric data archive (suada), Atmospheric Measurement Techniques, 7 (8), 2683-2694.

Guerova G., Tz. Dimitrova and S. Georgiev (2019), Thunderstorm Classification Functions Based on Instability Indices and GNSS IWV for the Sofia Plain, Remote sens., 11(24), 2988, https://doi.org/10.3390/rs11242988.

Hobiger T, Ichikawa R., Koyama Y., and Kondo T. (2008), Fast and accurate ray-tracing algorithms for real-time space geodetic applications using numerical weather models, Journal of Geophysical Research: Atmospheres, 113, D20302.

Hofmeister A. (2016), Determination of path delays in the atmosphere for geodetic VLBI by means of raytracing, PhD thesis. Department of Geodesy and Geoinformation, TU Wien.

Jiménez P. A., Dudhia J., González-Rouco J. F., Navarro J., Montávez, J. P., García-Bustamante, E. (2012), A revised scheme for the WRF surface layer formulation, Monthly Weather Review, 140(3), 898-918.

Kawabata Takuya, Shoji Yoshinori, Seko Hiromu, Saito Kazuo (2013), A Numerical Study on a Mesoscale Convective System over a Subtropical Island with 4D-Var Assimilation of GPS Slant Total Delays, Journal of the Meteorological Society of Japan, 91, p. 705-721. 10.2151/jmsj.2013-510.

Lim K. S. S., Hong, S. Y. (2010), Development of an effective double-moment cloud microphysics scheme with prognostic cloud condensation nuclei (CCN) for weather and climate models, Monthly weather review, 138(5), 1587-1612.

Mlawer E. J., Taubman S. J., Brown P. D., Iacono M. J., Clough S. A. (1997), Radiative transfer for inhomogeneous atmospheres: RRTM, a validated correlated-k model for the longwave. Journal of Geophysical Research: Atmospheres, 102(D14), 16663-16682.

Mircheva B., M. Tsekov, U. Meyer and G. Guerova (2020), Analysis of the 2014 Wet Extreme in Bulgaria: Anomalies of Temperature, Precipitation and Terrestrial Water Storage, Hydrology, 7(3), 66, https://doi.org/10.3390/hydrology7030066.

Stoycheva A., Markova B., Diakova A., Popova M., Kirilova A., Stoev K., Slavchev M., Tsekov G., Balabanova S., Koshnicharov G., et al. (2015), The 2014 floods and their conditions, Bul. J. Meteo&Hydro, 20 (5), 73–105.

Taszarek M., Allen J., Púčik T., Groenemeijer P., Czernecki B., Kolendowicz L., Lagouvardos K., Kotroni V., Schulz W. (2019), A climatology of thunderstorms across Europe from a synthesis of multiple data sources. J. Clim. , 32, 1813–1837.

Zamfirov I., Georgiev Ch. G., and Stoyanova J. (2014), Case study of two splitting hailstorms over Bulgaria on 20 May 2013, ERAD 2014 – The Eight European Conference on Radar in Meteorology and Hydrology.